Neuronal synchrony reveals working memory networks and predicts individual memory capacity

J. Matias Palva[a,1], Simo Monto[a,b,2], Shrikanth Kulashekhar[a,b,2], and Satu Palva[a,1]

[a]Neuroscience Center, 00014-University of Helsinki, Finland; and [b]BioMag Laboratory, HUSLAB, Helsinki University Central Hospital, FI-00029 HUS, Finland

Visual working memory (VWM) is used to maintain sensory information for cognitive operations, and its deficits are associated with several neuropsychological disorders. VWM is based on sustained neuronal activity in a complex cortical network of frontal, parietal, occipital, and temporal areas. The neuronal mechanisms that coordinate this distributed processing to sustain coherent mental images and the mechanisms that set the behavioral capacity limit have remained unknown. We mapped the anatomical and dynamic structures of network synchrony supporting VWM by using a neuro informatics approach and combined magnetoencephalography and electroencephalography. Interareal phase synchrony was sustained and stable during the VWM retention period among frontoparietal and visual areas in α- (10–13 Hz), β- (18–24 Hz), and γ- (30–40 Hz) frequency bands. Furthermore, synchrony was strengthened with increasing memory load among the frontoparietal regions known to underlie executive and attentional functions during memory maintenance. On the other hand, the subjects' individual behavioral VWM capacity was predicted by synchrony in a network in which the intraparietal sulcus was the most central hub. These data suggest that interareal phase synchrony in the α-, β-, and γ-frequency bands among frontoparietal and visual regions could be a systems level mechanism for coordinating and regulating the maintenance of neuronal object representations in VWM.

cortical synchrony | graph theory | magnetoencephalography | source modelling | functional connectivity

Functional MRI (fMRI) studies have shown that human visual working memory (VWM) is supported by neuronal activity in several cortical regions in the frontal, parietal, occipital, and temporal lobes (1–6), where the frontoparietal regions mediate attentional and central executive functions (2–4, 7, 8) and the visual areas underlie the formation of neuronal object representations (9–11) and sustain them in VWM (8). However, fMRI does not have the subsecond temporal precision required for revealing the neuronal mechanisms that integrate and coordinate the processing in the functionally distinct regions during VWM maintenance. These functions could be carried out by oscillatory synchrony (i.e., rhythmical millisecond-range temporal correlations of neuronal activity), which modulates neuronal interactions and regulates network communication (12–16). The functional role of oscillatory synchrony can be studied noninvasively by combining magnetoencephalography and electroencephalography (MEEG) recordings with source reconstruction techniques that reveal the anatomical structures producing the MEEG signals. Earlier studies have considered interactions among approximately three to nine cortical regions of interest and revealed attentional modulations of interareal synchrony (17–19). The interactions underlying VWM have remained uncharacterized. We hypothesized that neuronal synchronization is instrumental for the maintenance of object representations in VWM. To have this role, synchronization should be memory load-dependent, sustained and stable throughout the retention period, and correlated with the behavioral outcome (1). Synchronization should also be enhanced predominantly among those specific frontoparietal and visual structures that have previously been found to be active during VWM retention with

fMRI (1–6) and less among other possibly task-irrelevant brain regions. To address this hypothesis, we developed a neuroinformatics approach for mapping all recordable (~10^5) cortex-wide neuronal interactions (Fig. S1).

Results

VWM Task and Behavioral Performance. We used MEEG to record the ongoing brain activity of 13 subjects who performed a delayed match-to-sample VWM task (20) (Fig. 1A and *Materials and Methods*). On each trial, the subjects were presented a sample stimulus containing one to six colored squares, which they were instructed to memorize. One second later, a test stimulus appeared, and in 50% of trials, one square in the test had a different color than that square in the sample. The subjects indicated with a left or right thumb twitch whether or not the sample was identical to the test. The average response accuracy decreased from $99.0 \pm 0.4\%$ to $82.0 \pm 2.1\%$ (mean $\pm$ SEM; Fig. 1B), and the median reaction times increased from 560 ± 40 ms to 960 ± 90 ms (mean $\pm$ SEM) with the memory load increasing from one to six objects. In line with earlier data (20), the subjects' mean memory capacity was 4.1 ± 0.2 objects (mean $\pm$ SEM).

Interareal Phase Synchrony Is Memory Load-Dependent and Sustained During VWM Maintenance. We estimated the phase of single-trial ongoing neuronal activity in all cortical areas as a function of time and frequency by using wavelet filtering and a cortically constrained minimum norm estimate (MNE) (21). Neuronal interareal interactions were then quantified by evaluating phase synchrony (12) across trials for each pair of cortical areas and for each subject, time window, and frequency band. Statistically significant interareal interactions were represented as undirected graphs in which cortical areas are the vertices and significant interactions are the edges (22, 23) (Fig. 1C).

We first addressed whether the VWM retention period was associated with sustained and memory load-dependent interareal phase synchrony. In the average condition, we averaged phase synchrony data across the six memory load conditions and identified interactions that were significantly stronger than in the prestimulus level of the sample [Wilcoxon signed rank test: one-tailed alpha (A) level (A = 0.005) and false discovery rate (FDR) < 0.01]. In the load condition, we identified interactions for which the strength was positively correlated with the memory load (Spearman's rank correlation test: A = 0.005, FDR < 0.01). Task effects on phase synchrony were initially indexed at the graph level by using connection density, K, (Fig. 1C), which is the proportion of significant interareal interactions from all possible
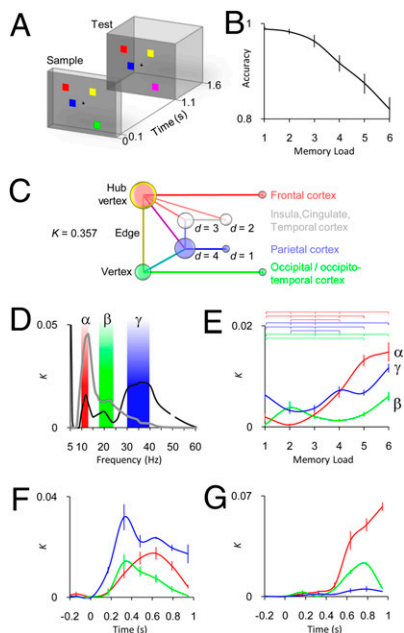
Fig. 1. Interareal phase synchrony in human cortex is robust, sustained, and memory load-dependent during VWM retention. (*A*) Example of a single experimental trial with a memory load of four and a test stimulus different from the sample stimulus. (*B*) Behavioral accuracy (mean ± SEM, n = 13) for the six memory load conditions. (*C*) Simplified graph showing the key graph theoretical concepts and the color code for Figs. 2–4. *d*, vertex degree that is the number of connections (edges) the vertex has; *K*, connection density, which in this study indicates the proportion of edges in the graph (here, statistically significant interactions: A = 0.005, FDR < 0.01) from all possible edges. (*D*) Mean *K* during the VWM retention period as a function of frequency for average (black line) and load (gray line) conditions. Interareal phase synchrony in α-, β-, and γ-frequency bands is stronger during VWM retention than during baseline (black line) and is strengthened by the memory load increasing from one to six objects (gray line). (*E*) *K* of retention period α- (red), β- (green), and γ- (blue) frequency band networks obtained separately for each memory load condition (mean ± SEM across 16 retention period graphs per frequency band). The horizontal lines indicate the memory load pairs with a significantly different *K* (P < 0.05, Bonferroni corrected, n = 15). (*F*) Average condition *K* as a function of time shows sustained network synchrony during the VWM retention period in the α-, β-, and γ-bands (mean ± SEM and colors as in *E*, SEM bars are at time window centers, VWM retention period includes the four time windows between 0.4 and 1 s). (*G*) Load condition *K* as a function of time (mean ± SEM and colors as in *E*).

(11,130) pairwise interactions among the 106 brain areas. The data showed that the VWM retention period (~0.4–1.1 s) was associated with memory load-dependent interareal synchrony in the alpha- (α, here 10–13 Hz), beta- (β, 18–24 Hz), and gamma- (γ, 30–40 Hz) frequency bands (Fig. 1*D*). We also evaluated *K* in each memory load condition separately for the α-, β-, and γ-frequency bands (Wilcoxon signed rank test: A = 0.005, FDR < 0.01), which showed that in addition to strengthening the phase synchrony (Fig. 1*D*), an increasing VWM load increased the number of significant interareal interactions (Fig. 1*E*; permutation test: P < 0.05, Bonferroni corrected).

We then asked whether the synchronized networks were sustained and stable throughout the entire retention period. An evaluation of *K* as a function of time showed that the network synchrony emerged soon after the onset of the sample stimulus in the α-, β-, and γ-frequency bands (Fig. 1*F*) and persisted throughout the VWM retention period both in the average (Fig. 1*F*) and load (Fig. 1*G*) conditions. The temporal stability of the anatomical structures of synchronized networks was tested by comparing different time windows with edge- and vertex-wise graph similarity indices (P < 0.01, Bonferroni corrected; Fig. S2

A–H), which showed that in both the average and load conditions, the α-, β-, and γ-band networks were, indeed, significantly similar throughout the retention period. Taken together, the network synchrony in the α-, β-, and γ-bands was robust, memory load-dependent, sustained, and temporally stable throughout the VWM retention period, and thus fulfills the criteria set forth in our hypothesis. Nevertheless, if interareal synchrony was to sustain neuronal object representations in VWM, synchronization should, in addition, be enhanced among task-relevant frontoparietal and visual structures (1–6).

Network Structures of α-, β-, and γ-Frequency Band Interactions in the Average Condition. We addressed the anatomical structure of the α-, β-, and γ-band networks by averaging into matching graphs (*SI Text*) the 16 binary graphs of the four retention period time windows and four wavelet frequencies that comprised each frequency band. Matching graphs are weighted graphs, given the mean of a set of binary graphs. Each edge value (the edge matching index, M^E) thus represents the fraction of graphs in which the edge was present. Hence, the matching graphs reveal the most common interareal interactions, which are likely to reflect important communication pathways. We also used vertex degree and betweenness centrality to identify brain areas that were network hubs. The degree is the number of edges that connect a vertex with other vertices (Fig. 1*C*). The vertex betweenness centrality, on the other hand, quantifies the fraction of the shortest paths in the graph that pass through the vertex (22). Nodes with high degree and betweenness centrality are crucial for efficient communication in the network. Fig. 2 shows the networks in the α-, β-, and γ-bands. The α-band network comprised orbitofrontal (orbital gyrus/sulcus), ventrolateral (inferior frontal gyrus/sulcus), and dorsolateral (middle frontal gyrus, superior frontal sulcus) prefrontal areas; premotor-motor (precentral gyrus/sulcus, central sulcus) areas, including the frontal eye fields (superior frontal sulcus, superior precentral sulcus); and areas in the parietal cortex and in occipito- and inferotemporal cortices (Fig. 2*A* and Fig S3*A*). Hubs were located to the frontal cortex both in the matching graph (Fig. 2*A* and Fig. S3*A*) and in the individual graphs (Fig. S3*B*). Compared with the α-band network, wherein the synchronization was most robust within hemispheres, the β-band network was largely interhemispheric and comprised visual areas in the occipital and occipitotemporal cortices (Fig. 2*B* and Fig. S3*C*). Major hubs were found in the right hemispheric extrastriate regions (superior occipital gyrus/sulcus, cuneus) and parietooccipital sulcus, as well as in the left hemispheric intraparietal sulcus and insula (anterior insula, posterior insula) (Fig. 2*B* and Fig. S3 *C and D*). The γ-band network was the strongest and encompassed many areas in the frontoparietal and visual regions (Fig. 2*C* and Fig. S3*E*). Similar to the β-band, the γ-band synchronization was also strong between the hemispheres. The intraparietal sulci in both hemispheres and the left hemispheric superior parietal gyrus were the most central hubs, but the superior occipital gyrus/sulcus and precuneus were also major hubs (Fig. 2*C* and Fig. S3 *E and F*). To identify the connections that were common across frequency bands, we performed a colocalization analysis by merging α-, β-, and γ-band graphs into a matching graph in which the edges were colored according to the frequency band. Although the colocalization analysis revealed that multiband connections were most pronounced among frontoparietal structures and that there was a greater proportion of β-γ-edges than expected by chance (compare Fig. S2 *E and F*), it also showed that the α-, β-, and γ-band networks were partially segregated along the anterior-posterior axis (Fig. S4 *A and B*). Thus, during VWM retention, the frontoparietal areas were bound predominantly by α- and γ-band phase synchrony, whereas the networks in the occipital, occipitotemporal, and parietal cortices were engaged in synchronized β- and γ-band oscillations.
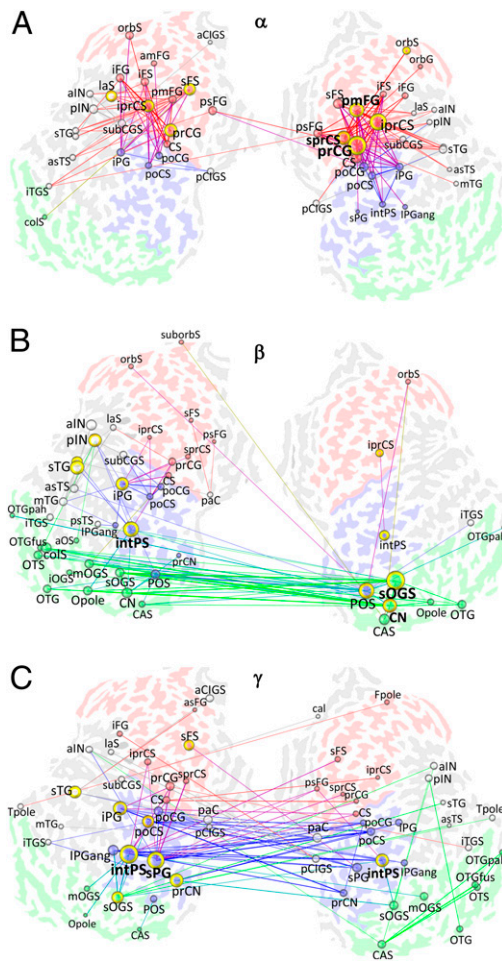
Fig. 2. Structure of interareal interactions mediated by phase synchrony in α-, β-, and γ-frequency bands during VWM retention. (A) α-Band matching graph ($M^E_{min} = 0.55$, details provided in Fig. S3A). A matching graph reveals spectrally and temporally stable interactions that are likely to underlie the most important communication pathways. The underlying map shows the complete left and right flattened cerebral hemispheres with sulci colored according to the cortical region (Fig. 1C). Lines indicate interareal interactions and are colored according to the connected brain regions. Spheres and annotations indicate brain areas, with radii proportional to their degree. Yellow borders encircle areas with betweenness centrality values in the top 10th percentile. Brain regions with a large degree and betweenness centrality are the network hubs. The bolding of annotations indicates the top three hubs in individual graphs (Fig. S3B). (B) β-Band (18–24 Hz) matching graph ($M^E_{min} = 0.3$; Fig. S3 C and D). (C) γ-Band (30–40 Hz) matching graph ($M^E_{min} = 0.5$; Fig. S3 E and F). C, central; CA, calcarine; CI, cingulate; CN, cuneus; F, frontal; G, gyrus; IN, insula; P, parietal; S, sulcus; T, temporal; O, occipital; a, anterior; ang, angular; cal, callosal; col, collateral; i, inferior; int, intra; ist, isthmus; fus, fusiform; la, lateral; m, middle; orb, orbital; p, posterior; pa, para; pah, parahippocampal; pla, planum temporale and polare; pe, peri; pr, pre; po, post; s, superior; tr, transverse.

Increasing Memory Load Strengthens Frontoparietal Phase Synchrony.
We then characterized the network structure of interactions that were positively correlated with an increasing memory load. In the α-band, these interactions were dense among the frontoparietal regions (Fig. 3A and Fig. S5A). In addition, this bilateral frontoparietal network was connected to the cingulate gyrus/sulcus, insula, and occipitotemporal cortex. Although several hubs were in the frontal cortex as in the average condition, the load condition networks also had highly central hubs in the postcentral sulcus and intraparietal sulcus (Fig. 3 and Fig. S5 A and B). In both β- and γ-bands, the increasing memory load strengthened
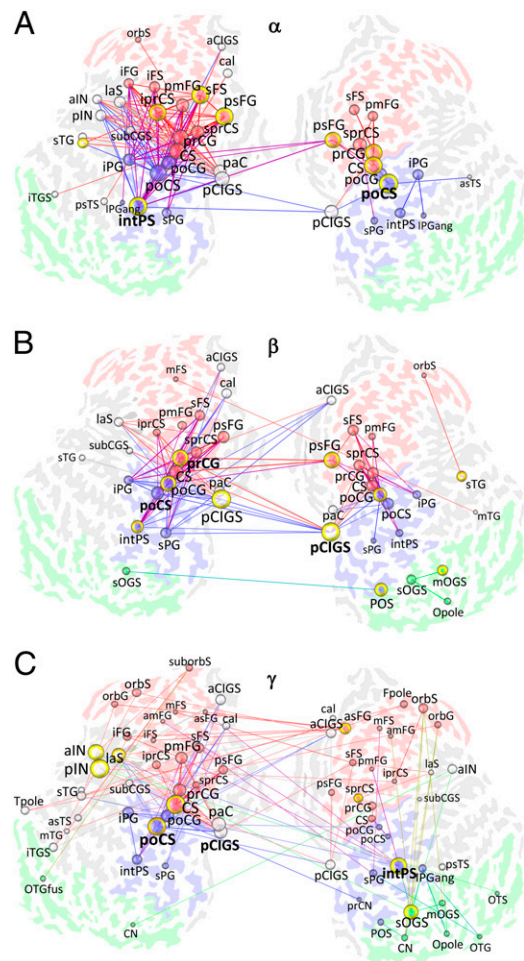
Fig. 3. Retention period phase synchrony is strengthened among frontoparietal and visual regions with increasing memory load. (A) α-Band matching graph. Visualization as in Fig. 2 ($M^E_{min} = 0.81$; Fig. S5 A and B). (B) β-Band matching graph ($M^E_{min} = 0.5$; Fig. S5C). (C) γ-Band matching graph ($M^E_{min} = 0.18$; Fig. S5E). C, central; CA, calcarine; CI, cingulate; CN, cuneus; F, frontal; G, gyrus; IN, insula; P, parietal; S, sulcus; T, temporal; O, occipital; a, anterior; ang, angular; cal, callosal; col, collateral; i, inferior; int, intra; ist, isthmus; fus, fusiform; la, lateral; m, middle; orb, orbital; p, posterior; pa, para; pah, parahippocampal; pla, planum temporale and polare; pe, peri; pr, pre; po, post; s, superior; tr, transverse.

phase synchrony among the visual regions, frontoparietal regions, posterior cingulate gyrus/sulcus, and insula (Fig. 3 B and C and Fig. S5 C and E). The most central hub in the β-band was the posterior cingulate gyrus/sulcus, with other hubs being in frontoparietal regions (Fig. 3B and Fig. S5 C and D). In the γ-band networks, the right hemispheric intraparietal sulcus was an important hub, and other hubs included the left hemispheric insula, postcentral sulcus, and central sulcus (Fig. 3C and Fig. S5 E and F). The α-β-γ-colocalization graph was dominated by frontoparietal α-interactions and colocalized α-β- and α-β-γ-interactions (Fig. S4 C and D). In contrast to the average condition, the colocalization revealed a higher number of α-β-γ-edges than expected by chance (Fig S4D). These data are thus in line with the robust graph-to-graph similarity between the α-, β-, and γ-frequency bands in the load condition (Fig. S2 G and H). Taken together, the characterization of the structure of memory load-dependent synchronization revealed the classic VWM network that is characterized by activity in the intraparietal sulcus, premotor and postcentral regions, frontal eye fields, and lateral prefrontal cortex.

Intraparietal Sulcus Is the Primary Hub in Networks That Predict Individual Behavioral VWM Capacity. The average and load condition data suggested that interareal interactions regulated by phase synchrony could be a systems level mechanism for sustaining neuronal object representations in VWM. To test this notion, we asked whether interareal synchrony would predict the subjects' behavioral VWM capacity. To have this role, phase synchrony should be strengthened with increasing memory load up to the individual VWM capacity but should level off thereafter (5, 24). We thus estimated for each interaction the memory load value at which the strength of phase synchrony plateaued and tested across subjects whether this value predicted the subjects' behavioral VWM capacity (Spearman's rank correlation test: $A = 0.025$, FDR < 0.01). Fig. 4 *A* and *B* shows that, indeed, network synchrony in the α- and β-bands predicted the individual VWM capacity, which led us to evaluate the cortical structures of these networks. In both bands, the networks were centered around the right and left intraparietal sulci, which were the primary hubs (Fig. 4 *C* and *D* and Fig. S6 *A–D*).

Discussion

Several prior studies have shown that the amplitudes of neuronal oscillations in the α-, β-, and γ-bands are modulated in VWM tasks, which suggests that these oscillations play a functional role in human VWM (25–30). In the present study, we asked whether these oscillations are also long-range synchronized across cortical regions during human VWM. We show here that interareal phase synchrony in the human brain was stable, sustained, and memory load-dependent throughout the VWM retention period. Moreover, VWM-related synchrony was strengthened among those frontal, parietal, and visual cortical structures that are known to be important for VWM retention (1–6). The mechanistic link between interareal neuronal synchronization and behavioral level VWM (cf. 5, 24, 31) is further supported by the discovery of networks in which the strength of phase synchrony predicted the individual psychophysical VWM capacity. Our results thus imply that long-range phase synchrony can be a systems level mechanism for the maintenance of neuronal object representations in VWM.

Although long-range synchrony has been detected during VWM maintenance among different electroencephalographic (EEG) electrodes (32) and during a working memory task among magnetoencephalographic (MEG) sensors (33), source reconstruction techniques have been used in only a few MEG studies. Prior studies exploiting inverse modeling have revealed attention-dependent cortical interareal synchrony (17–19). The present study characterizes cortical interareal interactions underlying VWM and also comprehensively maps phase-synchronized cortex-wide networks in source space without a limitation of the analysis to a small set of anatomy- or data-derived regions of interest. Our screening approach avoids the inferential problems associated with the limited number of regions of interest in source-space synchrony analyses (34) and the statistical inflation brought about by circular data inspection and selection of regions of interest (35).

In this study, the network hubs in the α-, β-, and γ-bands were located in those frontoparietal and visual regions that have previously been observed with fMRI recordings to be active during VWM retention (1–6). The present MEEG data thus constitute an independent rediscovery of the fMRI-mapped anatomical substrates of VWM retention, which validates our methodological approach and emphasizes the value of combined cortex-wide interaction mapping and graph analysis (22, 23). MEEG can thus complement fMRI in revealing the temporal, spectral, and anatomical structure of functional connectivity in subsecond time scales.

Working memory is thought to comprise attentional or central executive functions as well as sensory storage functions (36).
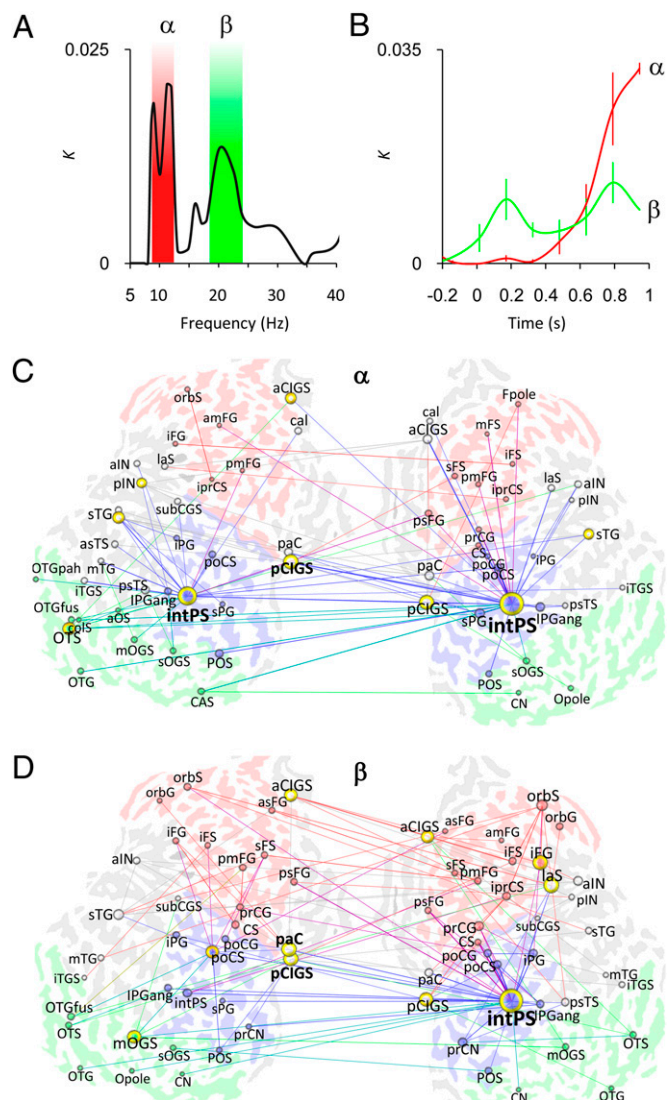

Fig. 4. Individual behavioral VWM capacity is predicted by α- and β-band networks in which the intraparietal sulcus is the most central hub. (*A*) *K* as a function of frequency shows that the interactions correlated with individual VWM capacity are concentrated to the α- (here, 9–12 Hz) and β-bands. (*B*) Dynamics of *K* of the α- and β-band networks (mean ± SEM across 16 retention period graphs per frequency band). (*C*) α-Band matching graph for the VWM retention period ($M^E_{min} = 0.35$; details provided in Fig. S6A). (*D*) β-Band matching graph ($M^E_{min} = 0.24$; Fig. S6C). C, central; CA, calcarine; CI, cingulate; CN, cuneus; F, frontal; G, gyrus; IN, insula; P, parietal; S, sulcus; T, temporal; O, occipital; a, anterior; ang, angular; cal, callosal; col, collateral; i, inferior; int, intra; ist, isthmus; fus, fusiform; la, lateral; m, middle; orb, orbital; p, posterior; pa, para; pah, parahippocampal; pla, planum temporale and polare; pe, peri; pr, pre; po, post; s, superior; tr, transverse.

fMRI studies show that these attentional and central executive functions arise in frontoparietal circuits (2–4, 7, 8) and suggest that the neuronal representations are sustained in VWM in visual cortical regions (8). In this study, the average condition revealed the VWM encoding- and retention-related strengthening of interareal phase synchrony from the level of ongoing presample stimulus activity. In the average condition, synchronous interactions involving the visual regions took place largely in the β- and γ-bands, which is in good agreement with the proposal that neuronal synchrony in this frequency range binds neuronal object representations (16). β- and γ-band synchronization also

involved the frontoparietal regions, but the α-band phase synchrony was most predominant there, which supports the idea that phase correlations in the β- and γ-bands (37–41), as well as in the α-band (42, 43), are related to attentional functions.

Increasing memory load, which is associated with enhanced attentional demands, strengthened interareal synchrony among the frontoparietal regions most strongly in the α-frequency band and to a lesser extent in the β- and γ-frequency bands. This suggests that frontoparietal α-, β-, and γ-band interactions are involved in regulation of the attentional top-down modulation (37–43) that drives the maintenance of object representations in VWM (8). Interestingly, the load-dependent synchronized frontoparietal networks were, to a considerable extent, uncorrelated with the VWM capacity, which points to the possibility that the synchronization among these regions could reflect progressive recruitment of additional processing resources at supracapacity memory loads. Furthermore, the average and load condition data imply that several partially distinct and spectrally distributed attentional networks support VWM maintenance. In agreement with this idea, there was a clear trend of α-band network hubs being more frontally located than those of β- or γ-band networks, which leads us to speculate that the α-band network underlies higher level attentional functions. The γ-band network, on the other hand, had prominent hubs in the right hemispheric parietal and extrastriate regions, and is thus well positioned to mediate visual attention (37–41). In addition to the frontoparietal regions, network hubs were observed in the insula, cingulate, and orbitofrontal structures. These regions have been suggested to form a cinguloopercular attention system that underlies the task set maintenance (44). In our data, cinguloopercular and orbitofrontal regions were synchronized both with visual and frontoparietal regions during VWM maintenance, suggesting that VWM retention is associated with concurrent activity in and phase interactions among distinct attentional systems (45). Taken together, these data suggest that neuronal coupling in the α-, β-, and γ-frequency bands may underlie partially distinct functions in VWM maintenance. In line with this idea, our recent study on graph properties of these interaction networks showed that the α- and β-band networks were memory load-dependently more clustered than those in the γ-band (46). Mechanisms underlying the integration of such anatomically and spectrally distributed networks remain unknown but could involve cross-frequency phase interactions (33, 42, 47–50).

The intraparietal sulcus was one of the principal hubs in both the average and load conditions. In the β- and γ-bands, the intraparietal sulcus also interconnected the visual and frontoparietal networks. This central position between the attentional and representational networks is intriguing in light of the dual functional roles that have been assigned to both the intraparietal sulcus (10, 51) and the β-γ-oscillations (16, 37) in visual attention and in forming visual object representations. Importantly, the intraparietal sulcus was the most central hub in networks predicting individual VWM capacity, which is in perfect agreement with recent fMRI data (5, 31) and also with EEG studies revealing VWM capacity-related event-related potentials (24) and oscillatory amplitude modulations (52) in posterior brain regions. We suggest that the topological position as an information flow bottleneck between the visual representation and frontoparietal attention networks is a key factor in the role of the intraparietal sulcus in limiting VWM capacity and might contribute to the detrimental behavioral consequences of parietal lesions.

Conclusions

This study shows that α-, β-, and γ-frequency band phase synchrony between frontal, parietal, and visual brain areas is sustained, stable, memory load-dependent, and behaviorally relevant during human VWM maintenance. Interareal phase

synchrony could thus be a systems level mechanism for coordinating and regulating the maintenance of neuronal object representations in VWM.

Materials and Methods

Task and Stimuli. The VWM experiment was a based on a delayed matching-to-sample task in which the subjects were presented with a sample stimulus that had to be sustained in working memory and then compared with a test stimulus (20) (Fig. 1A). The sample stimulus was presented for 0.1 s, and it was followed by a memory retention period of 1 s, after which the test stimulus was presented for 0.5 s. The interval between the onset of the test stimulus and the onset of the next trial's sample stimulus varied randomly from 2.5 to 3.5 s. The stimuli contained one, two, three, four, five, or six randomly located squares that corresponded to six memory loads, L_M ($L_M = 1 \ldots 6$). The experiment comprised a total of 2,000 randomly ordered trials, giving ~330 trials per L_M. The squares had clearly dissociable colors (white, black, blue, red, purple, green, and yellow). Before the onset of the sample stimulus, the subjects fixated on a cross that was located at the center of the screen. The stimuli were projected onto a screen placed at ~234 cm from the subject's eyes. The size of the stimulus area was 7.3° × 7.3°, and that of the squares was 0.65° × 0.65°. The minimum center-to-center distance between the squares was 2°.

After the onset of the test stimulus, the subjects indicated with a forced choice left- or right-hand thumb twitch whether the stimuli were the "same" or "different." After this primary response, the subjects indicated whether they felt sure about their response with a second "go/no-go" twitch of the same thumb.

Behavioral Performance. Accuracy (i.e., the proportion of correct responses from all responses) and reaction time were analyzed separately for each memory load. Individual VWM capacity was estimated with Pashler's procedure (53), wherein the capacity is given by a plateau value, k_P, that is obtained for each L_M. The k_P values are given by $k_P(L_M) = L_M \times (H - FA)(1 - FA)^{-1}$, where H is the proportion of correct different responses and FA is the proportion of incorrect different responses. The average and load condition analyses were based on artifact-free trials with correct behavioral responses (Fig. 1B), whereas the capacity condition analyses were based on all artifact-free trials.

Subjects and Recordings. Thirteen healthy right-handed volunteers participated in this study [28 ± 3 years of age (mean ± SD), 4 female]. Subjects had normal or corrected-to-normal vision. MEEG (366-channel) with 204 planar gradiometers, 102 magnetometers, and 60 EEG electrodes (Elekta Neuromag Ltd.) was recorded at 600 Hz throughout the experiment (Fig. S1A). The thumb-twitch responses were detected with electromyography of the abductor/flexor pollicis brevis, and the electrooculogram was used to detect ocular artifacts. Trials with the electrooculogram signal exceeding 50 μV were excluded from further analysis. The MaxFilter sofware (Elekta Neuromag Ltd.) was used to suppress extracranial noise and to colocalize the recordings in signal space. T1-weighted anatomical MRI scans for cortical surface models were obtained at a resolution of 1 × 1 × 1 mm or less with a 1.5-T MRI scanner (Siemens) (Fig. S1B). This study was approved by the Ethical Committee of Helsinki University Central Hospital and was performed according to the Declaration of Helsinki. Written informed consent was obtained from each subject before the experiment.

Data Analysis. A detailed description of the data analysis workflow is presented in *SI Text* and Fig. S1 and is briefly summarized here. Single-trial MEEG data were filtered with Morlet wavelets into 36 frequency bands ranging from 3 to 90 Hz. Complex cortically constrained MNEs were obtained from filtered trials and collapsed within a set of maximally independent cortical patches to estimate the phase of ongoing activity in each cortical patch. Pair-wise phase synchrony of each cortical patch with every other patch was then evaluated by computing the phase-locking value (*PLV*) across trials for each subject, time window, and frequency band. The *PLV* indexes the strength of phase locking irrespective of the mean phase difference. The phase synchrony matrices were baseline-corrected and compensated for the phase synchrony that was artifactually caused by cortical activity phase locked to the sample stimulus and were then morphed to a cortical parcellation that was common to all subjects. We also compared the inter-areal PLV values with the amplitude values to rule out the possibility that the results presented here would be caused by the signal-to-noise ratio modulations (see *SI Text*, and Fig. S7).

Group Statistics. The statistical significance of each pair-wise interaction was tested across the subject population for each experimental condition. In the average condition, the baseline and evoked synchrony-corrected *PLV* values

were tested against a null hypothesis of $PLV \leq 0$ using the Wilcoxon signed rank test (one-tailed $A = 0.005$ and FDR < 0.01). In the load condition, the $PLVs$ were obtained separately for $L_M = 1, 2, 3, 4, 5$, and 6 and then tested across subjects using the Spearman's rank correlation test against a null hypothesis that PLV (L_M) is uncorrelated or negatively correlated with L_M load (Spearman's rank correlation test: one-tailed $A = 0.005$, FDR < 0.01). The interactions predicting individual memory capacity were identified so that we obtained the $PLV(L_M)$ and searched the capacity value, k_L, that gave the best least-squares fit of the capacity function F_{cap} (L_M, g, k_L), where g indicates gain parameter, to $PLV(L_M)$ (*SI Text*). These best-fitting k_Ls were then tested across subjects with the Spearman's rank correlation test against the null hypothesis that k_Ls were uncorrelated or negatively correlated with the subjects' individual behavioral capacities, k_P (one-tailed $A = 0.025$, FDR < 0.01).

Graph Characterization. The statistical data were used as adjacency matrices for binary undirected graphs in which the cortical areas are the vertices and significant interactions are the edges (23). Network visualizations in Figs. 2–4 were based on retention period matching graphs that were obtained from 16 primary graphs [four time windows with centers at 450–980 ms after stimulus onset (Fig. 1) and four wavelet frequencies in each frequency band: $\alpha = 10$–13 Hz, $\beta = 18$–24 Hz, $\gamma = 30$–40 Hz]. To obtain visualizations that were comparable across frequency bands and experimental conditions, the matching graphs were thresholded with as high an edge-matching index as possible that gave a final $K \geq 0.1$ (Figs. S3, S5, and S6) or $K \geq 0.02$ (Figs. 2–4, see also Fig. S8). Vertex degree and betweenness centrality were used to identify network hubs in the matching graphs at $K \geq 0.1$ (classification at $K \geq 0.1$ was also used in Figs. 2–4) and in individual graphs (Figs. S3, S5, and S6).

1. Pessoa L, Gutierrez E, Bandettini P, Ungerleider L (2002) Neural correlates of visual working memory: fMRI amplitude predicts task performance. *Neuron* 35:975–987.
2. Prabhakaran V, Narayanan K, Zhao Z, Gabrieli JD (2000) Integration of diverse information in working memory within the frontal lobe. *Nat Neurosci* 3:85–90.
3. Rowe JB, Toni I, Josephs O, Frackowiak RS, Passingham RE (2000) The prefrontal cortex: Response selection or maintenance within working memory? *Science* 288:1656–1660.
4. Sakai K, Rowe JB, Passingham RE (2002) Active maintenance in prefrontal area 46 creates distractor-resistant memory. *Nat Neurosci* 5:479–484.
5. Todd JJ, Marois R (2004) Capacity limit of visual short-term memory in human posterior parietal cortex. *Nature* 428:751–754.
6. Linden DE, et al. (2003) Cortical capacity constraints for visual working memory: Dissociation of fMRI load effects in a fronto-parietal network. *NeuroImage* 20:1518–1530.
7. Petrides M (2005) Lateral prefrontal cortex: Architectonic and functional organization. *Philos Trans R Soc London B* 360:781–795.
8. Curtis CE, D'Esposito M (2003) Persistent activity in the prefrontal cortex during working memory. *Trends Cogn Sci* 7:415–423.
9. Bell AH, Hadj-Bouziane F, Frihauf JB, Tootell RB, Ungerleider LG (2009) Object representations in the temporal cortex of monkeys and humans as revealed by functional magnetic resonance imaging. *J Neurophysiol* 101:688–700.
10. Konen CS, Kastner S (2008) Two hierarchically organized neural systems for object information in human visual cortex. *Nat Neurosci* 11:224–231.
11. Riesenhuber M, Poggio T (2002) Neural mechanisms of object recognition. *Curr Opin Neurobiol* 12:162–168.
12. Womelsdorf T, et al. (2007) Modulation of neuronal interactions through neuronal synchronization. *Science* 316:1609–1612.
13. Cardin JA, et al. (2009) Driving fast-spiking cells induces gamma rhythm and controls sensory responses. *Nature* 459:663–667.
14. Lakatos P, Karmos G, Mehta AD, Ulbert I, Schroeder CE (2008) Entrainment of neuronal oscillations as a mechanism of attentional selection. *Science* 320:110–113.
15. Womelsdorf T, Fries P, Mitra PP, Desimone R (2006) Gamma-band synchronization in visual cortex predicts speed of change detection. *Nature* 439:733–736.
16. Singer W (2009) Distributed processing and temporal codes in neuronal networks. *Cognitive Neurodynamics* 3:189–196.
17. Gross J, et al. (2004) Modulation of long-range neural synchrony reflects temporal limitations of visual attention in humans. *Proc Natl Acad Sci USA* 101:13050–13055.
18. Kujala J, et al. (2007) Phase coupling in a cerebro-cerebellar network at 8-13 Hz during reading. *Cereb Cortex* 17:1476–1485.
19. Siegel M, Donner TH, Oostenveld R, Fries P, Engel AK (2008) Neuronal synchronization along the dorsal visual pathway reflects the focus of spatial attention. *Neuron* 60:709–719.
20. Luck SJ, Vogel EK (1997) The capacity of visual working memory for features and conjunctions. *Nature* 390:279–281.
21. Hämäläinen MS, Ilmoniemi RJ (1994) Interpreting magnetic fields of the brain: Minimum norm estimates. *Med Biol Eng Comput* 32:35–42.
22. Bullmore E, Sporns O (2009) Complex brain networks: Graph theoretical analysis of structural and functional systems. *Nat Rev Neurosci* 10:186–198.
23. Rubinov M, Sporns O (2009) Complex network measures of brain connectivity: Uses and interpretations. *NeuroImage*, doi:10.1016/j.neuroimage.2009.10.003.
24. Vogel EK, Machizawa MG (2004) Neural activity predicts individual differences in visual working memory capacity. *Nature* 428:748–751.
25. Busch NA, Herrmann CS (2003) Object-load and feature-load modulate EEG in a short-term memory task. *NeuroReport* 14:1721–1724.
26. Sauseng P, Klimesch W, Schabus M, Doppelmayr M (2005) Fronto-parietal EEG coherence in theta and upper alpha reflect central executive functions of working memory. *Int J Psychophysiol* 57:97–103.
27. Osipova D, et al. (2006) Theta and gamma oscillations predict encoding and retrieval of declarative memory. *J Neurosci* 26:7523–7531.

28. Tallon-Baudry C, Bertrand O, Peronnet F, Pernier J (1998) Induced gamma-band activity during the delay of a visual short-term memory task in humans. *J Neurosci* 18:4244–4254.
29. Jensen O, Gelfand J, Kounios J, Lisman JE (2002) Oscillations in the alpha band (9-12 Hz) increase with memory load during retention in a short-term memory task. *Cereb Cortex* 12:877–882.
30. Scheeringa R, et al. (2009) Trial-by-trial coupling between EEG and BOLD identifies networks related to alpha and theta EEG power increases during working memory maintenance. *NeuroImage* 44:1224–1238.
31. Xu Y, Chun MM (2006) Dissociable neural mechanisms supporting visual short-term memory for objects. *Nature* 440:91–95.
32. Sarnthein J, Petsche H, Rappelsberger P, Shaw GL, von Stein A (1998) Synchronization between prefrontal and posterior association cortex during human working memory. *Proc Natl Acad Sci USA* 95:7092–7096.
33. Palva JM, Palva S, Kaila K (2005) Phase synchrony among neuronal oscillations in the human cortex. *J Neurosci* 25:3962–3972.
34. Schoffelen JM, Gross J (2009) Source connectivity analysis with MEG and EEG. *Hum Brain Mapp* 30:1857–1865.
35. Kriegeskorte N, Simmons WK, Bellgowan PS, Baker CI (2009) Circular analysis in systems neuroscience: The dangers of double dipping. *Nat Neurosci* 12:535–540.
36. Baddeley A (1996) The fractionation of working memory. *Proc Natl Acad Sci USA* 93:13468–13472.
37. Womelsdorf T, Fries P (2007) The role of neuronal synchronization in selective attention. *Curr Opin Neurobiol* 17:154–160.
38. Fries P (2009) Neuronal gamma-band synchronization as a fundamental process in cortical computation. *Annu Rev Neurosci* 32:209–224.
39. Jensen O, Kaiser J, Lachaux JP (2007) Human gamma-frequency oscillations associated with attention and memory. *Trends Neurosci* 30:317–324.
40. Gregoriou GG, Gotts SJ, Zhou H, Desimone R (2009) High-frequency, long-range coupling between prefrontal and visual cortex during attention. *Science* 324:1207–1210.
41. Tallon-Baudry C (2009) The roles of gamma-band oscillatory synchrony in human visual cognition. *Front Biosci* 14:321–332.
42. Palva S, Palva JM (2007) New vistas for alpha-frequency band oscillations. *Trends Neurosci* 30:150–158.
43. Klimesch W, Sauseng P, Hanslmayr S (2007) EEG alpha oscillations: The inhibition-timing hypothesis. *Brain Res Rev* 53:63–88.
44. Dosenbach NU, Fair DA, Cohen AL, Schlaggar BL, Petersen SE (2008) A dual-networks architecture of top-down control. *Trends Cogn Sci* 12:99–105.
45. Gilbert CD, Sigman M (2007) Brain states: Top-down influences in sensory processing. *Neuron* 54:677–696.
46. Palva S, Monto S, Palva JM (2010) Graph properties of synchronized cortical networks during visual working memory maintenance. *NeuroImage* 49:3257–3268.
47. Schroeder CE, Lakatos P (2009) Low-frequency neuronal oscillations as instruments of sensory selection. *Trends Neurosci* 32:9–18.
48. Lisman JE, Idiart MA (1995) Storage of 7 +/− 2 short-term memories in oscillatory subcycles. *Science* 267:1512–1515.
49. Roopun AK, et al. (2008) Temporal interactions between cortical rhythms. *Frontiers in Neuroscience* 2:145–154.
50. Tort AB, et al. (2008) Dynamic cross-frequency couplings of local field potential oscillations in rat striatum and hippocampus during performance of a T-maze task. *Proc Natl Acad Sci USA* 105:20517–20522.
51. Bressler SL, Tang W, Sylvester CM, Shulman GL, Corbetta M (2008) Top-down control of human visual cortex by frontal and parietal cortex in anticipatory visual spatial attention. *J Neurosci* 28:10056–10061.
52. Sauseng P, et al. (2009) Brain oscillatory substrates of visual short-term memory capacity. *Curr Biol* 19:1846–1852.
53. Pashler H (1988) Familiarity and visual change detection. *Percept Psychophys* 44:369–378.